Contrib Mineral Petrol (2003) 145: 742–751
DOI 10.1007/s00410-003-0476-8

ORIGINAL PAPER

Wallace H. MacLean

The *'Profile'* method of calculating the composition of solid in magma fractionation, and its application to an alkaline volcano

Received: 5 April 2002 / Accepted: 3 April 2003 / Published online: 10 July 2003

Abstract A new *profile* mass balance procedure is presented to calculate the chemical composition of solid precipitated during cooling and crystallization of many tholeiitic and alkaline magmas. It is a variant of the earlier *interval* method (MacLean 2000, Contrib Mineral Petrol 139:85–100), and is also based on chemical variation diagrams of lava sequences (liquid profiles) constructed with a quantitative monitor of fractionation derived from the residual enrichment of an incompatible trace high field-strength element (HFSE). In this new *profile* method, the concentration of a component in solid is shown by mass transfer considerations to be a function of its mass on a liquid fractionation path (profile) and on a path (profile) of perfect incompatible enrichment. The latter hypothetically contains all of the component, hence subtraction of the amount contained in liquid will yield its mass in the solid. The calculations are straightforward and adaptable to both equilibrium and fractional crystallization processes. Corrections to the fractionation monitor for measured $D^{S/L}_{HFSE}$ (solid/liquid distribution coefficient), estimates of "trapped liquid" in solid, and other variables, can be applied. The method is illustrated with chemical data for a suite of alkaline volcanic rocks from Mt. Erebus, Antarctica (Kyle et al. 1992, J Petrol 33:849–875). The lavas are silica-undersaturated, and range from nepheline-bearing basanite to phonolite. The solids correspond to those of ultrabasic rocks through most of fractionation, and are more SiO_2-undersaturated than the lavas.

Editorial responsibility: I. Parsons

W. H. MacLean
Department of Earth and Planetary Sciences,
McGill University, 3450 University Avenue,
Montreal, Quebec, H3A 2A7, Canada
E-mail: whm@eps.mcgill.ca
Fax: +1-514-3984680

Introduction

Tholeiitic and alkaline magmas are largely generated in the mantle and cool and crystallize on their rise to the Earth's surface. Periodic eruption of lava provides samples of magma that can be used to follow the chemical evolution of the liquid, but it is not a simple matter to obtain chemical compositions of the coeval solids. Solids are accessible for study only if exhumed, or penetrated by drilling or other means, and, even in those circumstances, segregation, reworking of minerals, and other processes in magma chambers (Hunter 1996) may well make it extremely difficult to match coeval solids with individual lavas.

It seems intuitive, nevertheless, that if the chemical evolution of the liquid is known, that of the solid fraction should be amenable to calculation. The crux of the problem lies in evaluating the precise fraction of liquid (*F*) and solid (1-*F*) at all points of differentiation. Once this problem is resolved, estimation of the total solid composition is straightforward, and can be calculated with simple mass-balance techniques, which can be used to derive numerical solutions for both equilibrium and incremental crystallization.

An earlier procedure to estimate the composition of solid was demonstrated by MacLean (2000), in what I refer to now as the *interval* method. The *interval* method was based on the premise that a liquid A evolved to a liquid B and solid A-B over an interval of *F*. The compositions of the liquids were taken from binary chemical variation diagrams of a suite of lavas, and the mass of solid (1-*F*) at each point of fractionation was obtained by conversion of the concentration of an incompatible trace high field-strength element (HFSE) to *F* via the Rayleigh distillation equation (Rayleigh 1896). The bulk chemical composition of the solids, the only unknown, was then calculated.

The *profile* method presented here is a variant of the *interval* method, and yields identical results. The procedure also employs differentiation paths (profiles) for

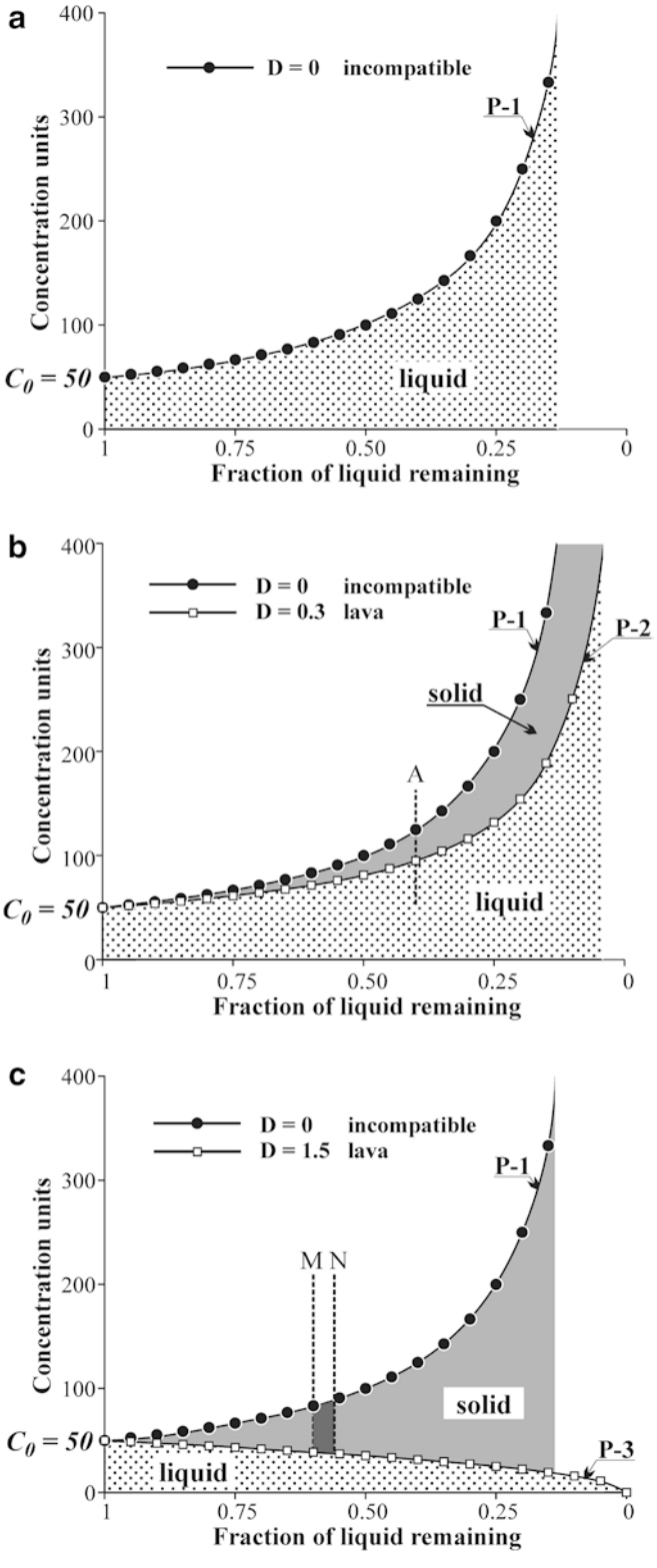

Fig. 1a–c Distribution of chemical components between liquid and solid with decreasing fraction of liquid. (F = fraction of liquid remaining). **a** Rayleigh incompatible enrichment ($D_i^{S/L} = 0$) for a component of liquid (P-1 profile). $C_o = 50$ is the starting concentration. All of the component is stored in liquid. **b** The distribution of a component with $D_i^{S/L} = 0.3$ (P-2 profile) between liquid and solid. The area below P-2 is the mass of the component in the liquid, and the area between P-1 and P-2 is its mass in the solid. *Line A* at $F = 0.4$ refers to calculations in the equilibrium crystallization model in Table 1a. **c** The distribution of a strongly compatible component with $D_i^{S/L} = 1.5$ (P-3 profile) between liquid and solid. The interval of F between M and N refers to calculations in the fractional crystallization model in Table 1b

oxides (and other components of the silicate liquid) on chemical variation diagrams monitored with F. A path (profile) of perfect incompatible enrichment is added for each component to hypothetically and independently store the entire mass of the oxide during fractionation. The mass of the component in the liquid is subtracted from the hypothetical incompatible mass to obtain its mass in solid. The procedure offers a unique visualization of the distribution of components between liquid and solid in a crystallizing magma, and provides a simple mass-balance method of calculation.

Enrichment of incompatible HFSE (Zr, Nb, Th, Hf, etc.) in liquid has been used to monitor differentiation in a variety of tholeiitic and alkaline lava suites (e.g., Barrett et al. 2001; MacLean 1990, 2000, MacLean and Barrett 1993). Once incompatibility of the HFSE has been established for a suite of lavas, accuracy in the calculation of solids depends largely on the closeness of samples to liquid compositions and the precision of fractionation trends. Contrary to the tholeiitic and alkaline liquids, the HFSE are compatible in most calc-alkaline and continental alkaline liquids, and thus do not yield reliable estimates of F.

Solids formed during the crystallization of tholeiitic magma were illustrated using the *interval* method of calculation (MacLean 2000). A suite of alkaline lavas from Mount Erebus, Antarctica (Kyle et al. 1992) has been chosen to illustrate the *profile* method. The Erebus lavas have penetrated continental crust, but the HFSE have remained incompatible and are used to calculate F. Plots of chemical compositions and normative minerals provide a clear history of the generation of solids in the middle to late stages of liquid evolution at this active volcano.

Rationale of the *profile* method

The principle of the *profile* method is illustrated in Fig. 1. The *"profiles"* are chemical variation diagrams (differentiation trends or paths) of components (oxides and trace elements) in a suite of lavas plotted against F, or the derived "% fractionated" [(1-F)*100] monitor. P-1 (Fig. 1a) is a hypothetical profile of perfect incompatible enrichment of a component. Profile P-2 (Fig. 1b) is a chemical fractionation trend for the same component in liquid, as established on a chemical variation diagram (monitored by *F)* for a suite of lavas exhibiting a range in chemical composition. It is apparent that the area between P-1 and P-2 represents the amount of the component in solid. The crux of the calculation is the estimation of F.

Estimation of F

The values of F are based on the residual enrichment of an incompatible HFSE in an evolving magma that periodically erupted a suite of lavas. That is, as a body of liquid solidifies, the incompatible element is concentrated in the decreasing mass of liquid. The incompatibility of the HFSE is well known in tholeiitic and many alkaline lava suites (MacLean 2000 and references therein), and measured distribution coefficients (mineral/liquid) are generally $D^{M/L}_{HFSE} < 0.1$ (Dalpé et al. 1995; Beattie 1994; Dunn and Sen 1994; Hack et al 1994; Mahood and Stimac 1990). Incompatibility throughout a span of fractionation is confirmed by the linearity of binary plots of the HFSE in collected samples of lava. Zr is the most abundant, and most commonly used, of these trace elements.

A value of F is calculated for each sample of lava by substituting its Zr content in the Rayleigh distillation equation (Rayleigh 1896):

$$c^l_{Zr} = c^o_{Zr} \bullet F^{D-1} \tag{1}$$

where c^l_{Zr} is the concentration of Zr in a sample of lava, c^o_{Zr} its original value in the lava suite (lowest Zr content of the lava samples), F is the fraction of liquid remaining, and $D^{S/L}_{Zr}$ (the bulk solid/liquid distribution coefficient) is initially set at zero. When measured values of $D^{S/L}_{Zr}$ are available, they can be substituted in the Rayleigh equation. F is the sole unknown, and is computed for each value of c^l_{Zr}, that is, for each chemically analyzed sample of the lava suite. The values of F are relative to the chosen value of c^o_{Zr}. Changes in the values of F are then used to monitor the chemical variation diagrams of the oxides and trace elements. Each scale unit of F represents an equal mass of liquid converted to solid.

Calculation of solid

The amount of an oxide (or other component) precipitated as solid is calculated from the separation of its incompatible enrichment and liquid chemical variation profiles, again using the example in Fig. 1b. It is calculated initially as mass and then converted to chemical concentration. The incompatible enrichment of mass (P-1) is generated with the Rayleigh equation:

$$m^l_i = m^o_i \bullet F^{D-1} \tag{2}$$

m^l_i is the incompatibly generated mass of the component in liquid, m^o_i its original or 'starting' mass, and F the fraction of liquid.

The P-2 profile is a chemical variation diagram for the component and generated here with $D^{S/L}_{oxide} = 0.3$; its origin is also m^o_i, and P-2 will lie below P-1. It is evident that the space between P-1 and P-2 represents the mass of the oxide in the crystallized solids (or immiscible liquid, vapor, etc., in special cases).

Mass-balance calculations

Mass-balance calculations, after the methods of Albarède (1995), are used to convert the masses of solid between P-1 and P-2 (Fig. 1b) into chemical compositions, and also to link the calculation procedures in the *profile* and *interval* methods. The chemical components at each value of F are processed individually and summed to obtain a bulk chemical composition of the solid. Since the mass of a component is conserved in a fractionating system, its total mass in liquid and solid (m^s_i) at a value of F is equal to its mass in the starting liquid:

$$m^o_i = m^l_i + m^s_i \tag{3}$$

The mass of a component is also a function of F and of its concentration (wt%, ppm, etc.) in liquid (c^l_i) and in solid (c^s_i):

$$m^l_i = F \bullet c^l_i, \text{and, since} F_o = 1, \tag{4}$$

$$m^s_i = (1 - F) \bullet c^s_i \tag{5}$$

hence, from Eq. (3):

$$1 \bullet c^o_i = F \bullet c^l_i + (1 - F) \bullet c^s_i \tag{6}$$

and

$$c^o_i = F \bullet c^l_i + (1 - F) \bullet c^s_i \tag{7}$$

This is equivalent to Eq. (1) in the *interval* method (MacLean 2000). Dividing through by F yields:

$$\frac{c^o_i}{F} = c^l_i + \frac{(1 - F)}{F} \bullet c^s_i \tag{8}$$

From Eq. (1), at $D = 0$,

$$c^o_i \bullet F^{-1} = \frac{c^o_i}{F} = c^{inc}_i \tag{9}$$

where c^{inc}_i is the perfectly incompatible enrichment concentration of the oxide, and Eq. (8) becomes:

$$c^{inc}_i = c^l_i + \frac{1 - F}{F} \bullet c^s_i \tag{10}$$

Thus, a mathematical relationship is developed to relate the hypothetical perfect incompatible build-up of a component to its concentration in liquid and in solid. The chemical composition of the solid is calculated for two types of magma solidification: (1) a process of *equilibrium* crystallization wherein solids and liquid continually equilibrate with each other as F decreases, and (2) a multistep *fractional* crystallization process wherein the solids are produced in narrow segments or 'fractions' of F, and preserved thereafter from reaction with liquid.

Equilibrium crystallization

In the *equilibrium* model a bulk composition is calculated for all components of solid from the start of

crystallization (F_o) of liquid to a value of F (MacLean 2000). It is the 'total solid composition' (TSC) of Morse (1997), and the simplest to visualize when a component follows a path of Rayleigh enrichment in the liquid (Fig. 1b). Rearrangement of Eq. (10) yields the chemical composition of a component of solid at a value of F:

$$c_i^s = \frac{F}{1-F} \cdot \left(c_i^{inc} - c_i^l\right) \tag{11}$$

Vertical line A at $F = 0.4$ in Fig. 1b represents a stage of F, with intersections on P-1 (c_i^{inc}) and P-2 (c_i^l); c_i^s is the bulk chemical composition of this component of solid produced between $F = 1$ and $F = 0.4$. Figure 1c illustrates stronger precipitation of a component at $D_i^{S/L} = 1.5$ (close to that of MgO and CaO in lava), producing areas that become much larger for solid than for liquid. Solidification with varying $D_i^{S/L}$ is calculated in the same way. For example, the profile of liquid evolution for TiO_2 in Fig. 2 follows a Rayleigh enrichment trend at $D_{TiO2}^{S/L} = 0$ in basalt, and a varying one at $D_{TiO2}^{S/L} > 1$ thereafter. A sample calculation is provided for a component of equilibrium crystallization of liquid in Table 1a. The procedure is repeated for each major oxide to obtain the bulk chemical composition of the solid.

Fractional crystallization

The fractional crystallization model calculates the bulk chemical composition of solids produced in narrow sequential 'fractions' of F (ΔF), wherein each fraction of new solid is isolated from reaction with liquid. As ΔF approaches zero, it becomes equivalent to the 'instantaneous solid composition' (ISC) of Morse (1997). Each ΔF segment has a new 'starting liquid' chemical composition (that at the end of the previous segment), and the composition of each component of solid is calculated

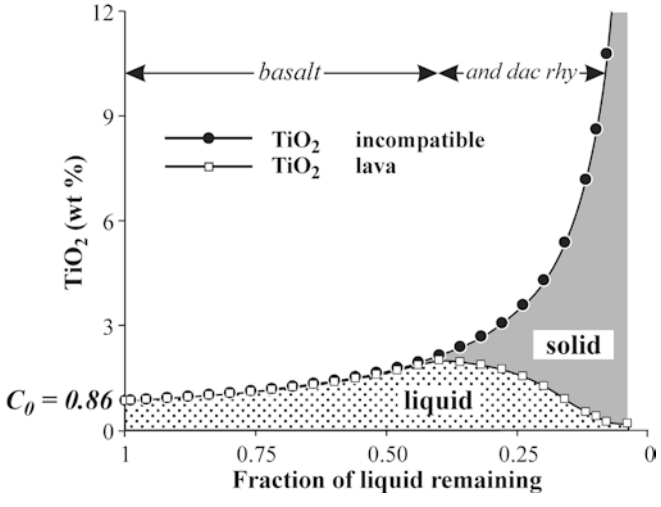

Fig. 2 Fractionation of TiO_2 in tholeiitic lava (MacLean 2000). TiO_2 is incompatibly enriched ($D_{TiO2}^{S/L} = 0$) in the basalt, but is compatible ($D_{TiO2}^{S/L} > 1$) and depleted in andesite (*and*), dacite (*dac*), and rhyolite (*rhy*)

only for ΔF (Fig. 1c). Mass-balance considerations define the chemical composition of the crystallized (in this case 'fractionated') solid in a segment (F_{MN}, Fig. 1c):

$$m_{i_{MN}}^s = m_{i_N}^s - m_{i_M}^s \tag{12}$$

Using the relations between m, c and F in Eqs. (3) and (4), this expands to:

$$(F_M - F_N) \bullet c_{i_{MN}}^s = (1 - F_N) \bullet c_{i_N}^s - (1 - F_M) \bullet c_{i_M}^s \tag{13}$$

where $c_{i_{MN}}^s$ represents the chemical composition of a component of solid generated between points of fractionation F_M and F_N, and $c_{i_M}^s$ and $c_{i_N}^s$ are the compositions of all solid formed up to the M and N values of F. Substituting Eq. (11) for each of these c_i^s values introduces the hypothetical incompatible enrichment profiles to the equation:

$$(F_M - F_N) \bullet c_{MN}^s = (1 - F_N) \bullet \frac{F_N}{1 - F_N} \bullet \left(c_{i_N}^{inc} - c_{i_N}^l\right) - (1 - F_M) \bullet \frac{F_M}{1 - F_M} \bullet \left(c_{i_M}^{inc} - c_{i_M}^l\right) \tag{14}$$

where $c_{i_M}^l$ and $c_{i_N}^l$ are the chemical compositions of the liquids at F_M and F_N.

Rearranging yields:

$$c_{i_{MN}}^s = \frac{1}{F_M - F_N} \bullet \left[F_N \bullet \left(c_{i_N}^{inc} - c_{i_N}^l\right) - F_M \bullet \left(c_{i_M}^{inc} - c_{i_M}^l\right)\right] \tag{15}$$

Thus, the composition of *fractionally crystallized* solid is directly related to the concentrations of components on incompatible enrichment and liquid chemical variation profiles. In the example in Fig. 1c, the component is being strongly depleted in liquid at $D_i^{S/L} = 1.5$. The procedure is repeated for each segment of fractionation. As the size of the segment diminishes, the process approaches perfect fractional crystallization

Table 1 The concentration of FeO in solid calculated with the *profile* method. Data are from Table 2 in wt%

(a) *Equilibrium* crystallization (Eq. 8), $F = 0.4$			
$\frac{F}{1-F}$	0.4/(1–0.4)	0.667	
c_i^{inc}			29.56
c_i^l			5.97
$c_i^{inc} - c_i^l$			23.59
c_i^s	23.59×0.667		15.73 wt%
(b) *Crystal fractionation* (Eq. 13), $\Delta F = 0.44$–0.40			
	F_N		F_M
F	0.40		0.44
c_i^{inc}	29.56		26.87
c_i^l	5.97		6.58
$c_i^{inc} - c_i^l$	23.59		20.29
xF	9.44		8.93
Difference		0.506	
ΔF	0.04		
c_i^s	0.506÷0.04		12.65 wt%

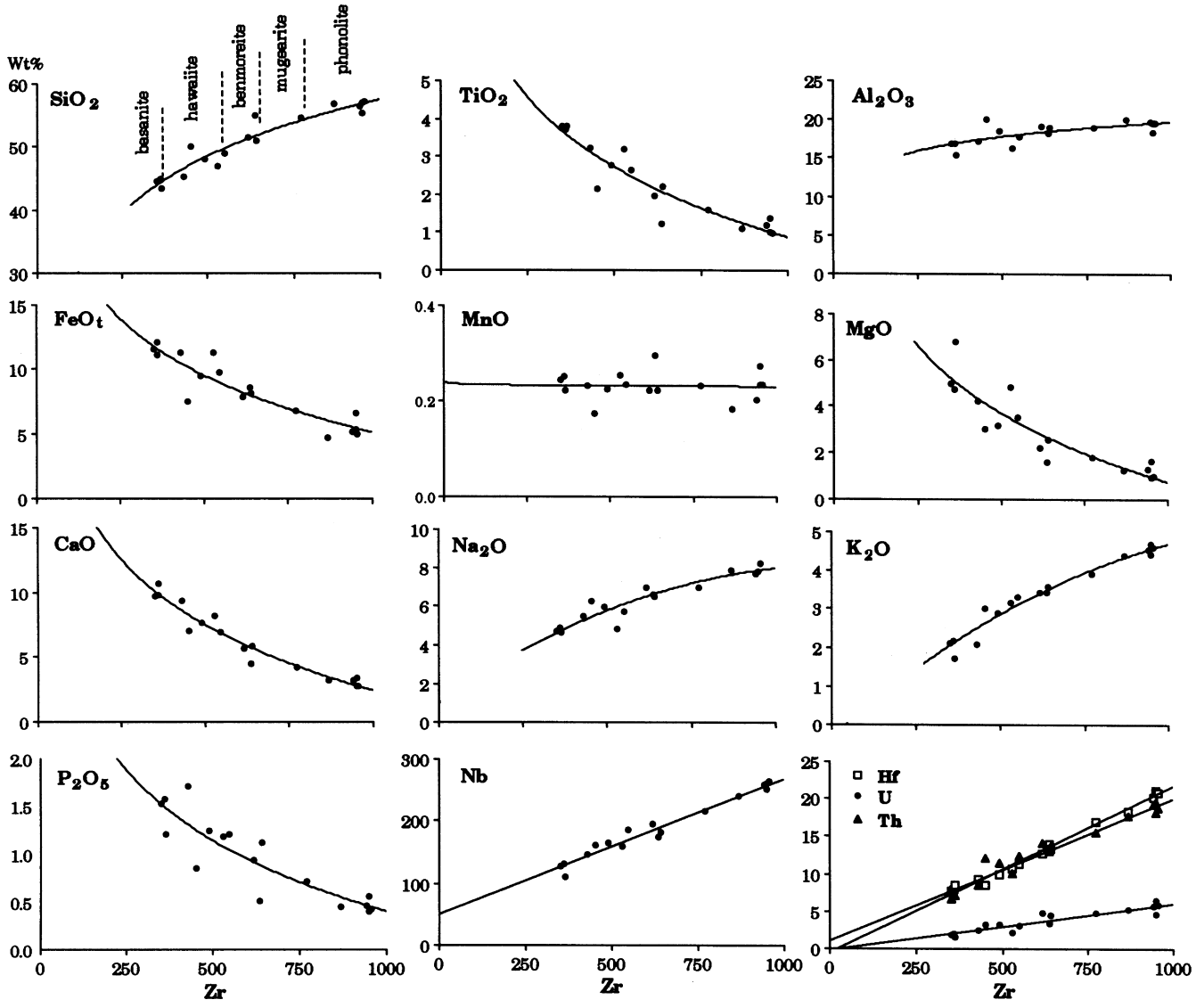

Fig. 3 Chemical variation diagrams (profiles) monitored with Zr for components of the Mt. Erebus lavas. The span of fractionation in the suite is from 350–1,000 ppm Zr. Samples of each lava type are from Kyle et al. (1992) and are shown on the SiO_2-Zr plot. Least-squares regression differentiation lines are fitted to the data

(ISC of Morse 1997). A sample calculation is given in Table 1b.

Equation (15) is directly related to Eq. (3) of the *interval* method. The bracketed portion can be rearranged into liquid and incompatible compositions:

$$c^s_{i_{MN}} = \frac{1}{F_M - F_N} \bullet \left[\left(F_N \bullet c^l_{i_N} - F_M \bullet c^l_{i_M}\right) - \left(F_N \bullet c^{inc}_{i_N} - F_M \bullet c^{inc}_{i_M}\right)\right] \quad (16)$$

The $F \bullet c^{inc}_i$ factors represent c^o_i in both cases, and cancel each other, leaving

$$c^s_{i_{MN}} = \frac{1}{F_M - F_N} \bullet \left(F_N \bullet c^l_{i_N} - F_M \bullet c^l_{i_M}\right) \quad (17)$$

which is equivalent to Eq. (3) in MacLean (2000). The input for Eq. (17) is simply the chemical compositions of the liquids at ends of the segment, $c^l_{i_M}$ and $c^l_{i_N}$, the values for F_M and F_N, and the outcome is the instantaneous solid composition (ISC) of Morse (1997).

Mt. Erebus alkaline lavas

The *profile* procedure is illustrated with chemical data from a suite of alkaline lavas from Mt. Erebus, Ross Island, Antarctica (Kyle et al. 1992). These data are used solely to portray the application of the *profile* method to the study of fractionated suites of lava. The lavas at Mt. Erebus are, in general, fresh, contain abundant incompatible HFSE, and exhibit an extended span of fractionation.

Mt. Erebus is a recently active alkaline, intraplate volcano with exposed nepheline-bearing lavas ranging from basanite to hawaiite, benmoreite, mugearite and anorthoclase phonolite (Kyle et al. 1992). According to

Table 2 Chemical compositions of liquids and solids derived from data of Kyle et al. (1992) for Mt. Erebus alkaline lavas

Liquid wt% (from chemical variation profiles of lavas)																		
SiO_2	43.92	44.05	44.47	45.03	45.62	46.24	46.88	47.55	48.26	49.00	49.79	50.62	51.50	52.45	53.48	54.61	55.86	57.29	57.68
TiO_2	3.67	3.64	3.56	3.45	3.33	3.21	3.08	2.94	2.80	2.65	2.49	2.31	2.13	1.93	1.72	1.49	1.23	0.95	0.88
Al_2O_3	16.82	16.85	16.94	17.06	17.19	17.32	17.46	17.60	17.75	17.91	18.08	18.25	18.44	18.63	18.85	19.09	19.36	19.66	19.75
FeO_t	11.82	11.76	11.57	11.30	11.02	10.72	10.41	10.08	9.74	9.37	8.98	8.57	8.12	7.65	7.14	6.58	5.97	5.30	5.13
MnO	0.23	0.23	0.23	0.23	0.23	0.23	0.23	0.23	0.23	0.23	0.23	0.23	0.23	0.23	0.23	0.23	0.23	0.23	0.23
MgO	5.21	5.16	5.04	4.86	4.67	4.47	4.27	4.05	3.82	3.58	3.32	3.05	2.76	2.44	2.10	1.73	1.33	0.89	0.77
CaO	10.12	10.04	9.82	9.51	9.19	8.85	8.50	8.12	7.73	7.31	6.86	6.39	5.88	5.34	4.75	4.12	3.42	2.65	2.45
Na_2O	4.62	4.65	4.75	4.88	5.02	5.17	5.33	5.51	5.69	5.89	6.10	6.33	6.58	6.84	7.11	7.40	7.68	7.95	8.01
K_2O	2.06	2.08	2.14	2.23	2.33	2.44	2.55	2.67	2.80	2.95	3.10	3.27	3.45	3.66	3.87	4.11	4.37	4.63	4.70
P_2O_5	1.52	1.51	1.48	1.44	1.39	1.34	1.29	1.23	1.17	1.11	1.05	0.98	0.91	0.83	0.74	0.65	0.55	0.43	0.40
Zr	350	354	365	380	398	417	438	461	486	515	547	583	625	673	729	795	875	972	1000
F[a]	1	0.99	0.96	0.92	0.88	0.84	0.8	0.76	0.72	0.68	0.64	0.6	0.56	0.52	0.48	0.44	0.4	0.36	0.35
Incompatible enrichment of oxides																			
SiO_2	43.92	44.36	45.75	47.74	49.91	52.29	54.90	57.79	61.00	64.59	68.62	73.20	78.43	84.46	91.50	99.82	109.80	122.00	125.49
TiO_2	3.67	3.71	3.82	3.99	4.17	4.37	4.59	4.83	5.10	5.40	5.74	6.12	6.55	7.06	7.65	8.34	9.18	10.20	10.49
Al_2O_3	16.82	16.99	17.53	18.29	19.12	20.03	21.03	22.14	23.37	24.74	26.29	28.04	30.04	32.35	35.05	38.24	42.06	46.73	48.07
FeO_t	11.82	11.94	12.32	12.85	13.44	14.08	14.78	15.56	16.42	17.39	18.47	19.71	21.11	22.74	24.63	26.87	29.56	32.84	33.78
MnO	0.23	0.23	0.24	0.25	0.26	0.28	0.29	0.31	0.32	0.34	0.36	0.39	0.41	0.45	0.48	0.53	0.58	0.64	0.66
MgO	5.21	5.26	5.42	5.66	5.92	6.20	6.51	6.85	7.23	7.66	8.14	8.68	9.30	10.01	10.85	11.83	13.02	14.46	14.88
CaO	10.12	10.22	10.54	11.00	11.50	12.04	12.65	13.31	14.05	14.88	15.81	16.86	18.07	19.46	21.08	22.99	25.29	28.10	28.91
Na_2O	4.62	4.67	4.81	5.02	5.25	5.50	5.78	6.08	6.42	6.80	7.22	7.70	8.25	8.89	9.63	10.51	11.56	12.84	13.21
K_2O	2.06	2.08	2.14	2.24	2.34	2.45	2.57	2.71	2.86	3.03	3.22	3.43	3.68	3.96	4.29	4.68	5.15	5.72	5.88
P_2O_5	1.52	1.54	1.59	1.66	1.73	1.81	1.90	2.00	2.12	2.24	2.38	2.54	2.72	2.93	3.17	3.46	3.81	4.23	4.35
Fractionated solid (wt%)																			
SiO_2		30.59	30.88	31.41	32.04	32.70	33.39	34.11	34.86	35.64	36.46	37.32	38.22	39.15	40.11	41.09	42.08	43.02	43.57
TiO_2		6.29	6.24	6.14	6.04	5.92	5.80	5.67	5.54	5.39	5.24	5.07	4.89	4.70	4.49	4.27	4.02	3.75	3.57
Al_2O_3		13.94	14.00	14.13	14.27	14.42	14.58	14.74	14.91	15.09	15.27	15.46	15.65	15.85	16.04	16.24	16.42	16.57	16.65
FeO_t[b]		18.08	17.96	17.75	17.49	17.22	16.93	16.63	16.31	15.96	15.59	15.20	14.77	14.31	13.81	13.26	12.65	11.98	11.53
MnO		0.23	0.23	0.23	0.23	0.23	0.23	0.23	0.23	0.23	0.23	0.23	0.23	0.23	0.23	0.23	0.23	0.23	0.23
MgO		9.37	9.15	8.97	8.79	8.59	8.39	8.17	7.94	7.69	7.43	7.15	6.84	6.51	6.15	5.76	5.33	5.05	
CaO		17.31	17.17	16.92	16.62	16.30	15.97	15.62	15.24	14.84	14.42	13.96	13.48	12.95	12.38	11.75	11.07	10.33	9.83
Na_2O		1.62	1.65	1.70	1.77	1.85	1.94	2.05	2.17	2.31	2.47	2.67	2.91	3.19	3.54	3.98	4.54	5.28	5.84
K_2O		0.01	0.03	0.05	0.09	0.13	0.18	0.24	0.30	0.37	0.46	0.57	0.69	0.85	1.03	1.27	1.57	1.95	2.25
P_2O_5		2.57	2.55	2.52	2.47	2.43	2.38	2.33	2.27	2.21	2.15	2.09	2.01	1.94	1.85	1.76	1.66	1.55	1.48

[a]Fraction of liquid remaining
[b]Total iron as FeO

these authors, they represent an intermediate to late-stage span of fractionation, and have low uniform $^{87}Sr/^{86}Sr$ indicating a lack of significant crustal contamination. The suite was chosen for its range of lava types, coherence of binary plots of the HFSE, and smooth fractionation trends for the oxides and HFSE (Fig. 3). The sorting of samples with the Zr monitor (Fig. 3, SiO_2-Zr) yields a basic-to-felsic trend of lava chemical evolution, without obvious gaps, and like that obtained by Kyle et al. using the SiO_2 monitor. The reason for the similarity is evident in the curvilinear correlation between Zr and SiO_2 in this span of fractionation (Fig. 3).

Only lavas from the main edifice of Mt. Erebus were used in the present study (EL—Erebus Lineage—lavas, Table 4 of Kyle et al. 1992). Plots of Zr against Th, U, Hf and Nb are linear and, except for Nb (discussed later), pass close to the origin (Fig. 3). The Zr/Nb value, a reasonably good indicator of alkalinity in intraplate lavas (e.g., Hofmann 1988), is ~3 for the suite, and similar to alkaline lavas at Tenerife, Canary Islands (~5, Ablay et al. 1998), Pantelleria, Italy (~6, Civetta et al. 1998) and Terceira, Azores (~7, Mungall and Martin 1995). Zr/Nb values are much higher in tholeiitic lavas: ~30 in MORB Leg 163 (Larson et al. 1999), and ~20 for Archean lavas at Matagami, Quebec (MacLean 2000).

Oxides versus Zr

The increasing concentration of Zr in the Mt. Erebus lavas sorts them in order of least to most differentiated. All these lavas are moderately silica-undersaturated, and K_2O contents range up to ~5 wt%, generating copious anorthoclase phonolite (Kyle et al. 1992). Plots of the major oxides versus Zr produce smooth and continuous fractionation trends over the range of ~350–1,000 ppm Zr (Fig. 3). The 350 ppm low value for Zr is the starting c^o_{Zr} value for calculation of F for the suite. Regression equations fitted to the sample arrays were used to obtain continuous chemical profiles of liquid evolution (Table 2). They display continuous enrichment of SiO_2, Al_2O_3, Na_2O and K_2O, and rather strong depletion of other oxides. The most basic basanite in this group of samples would be at or just beyond the peaks of Fe, Ti

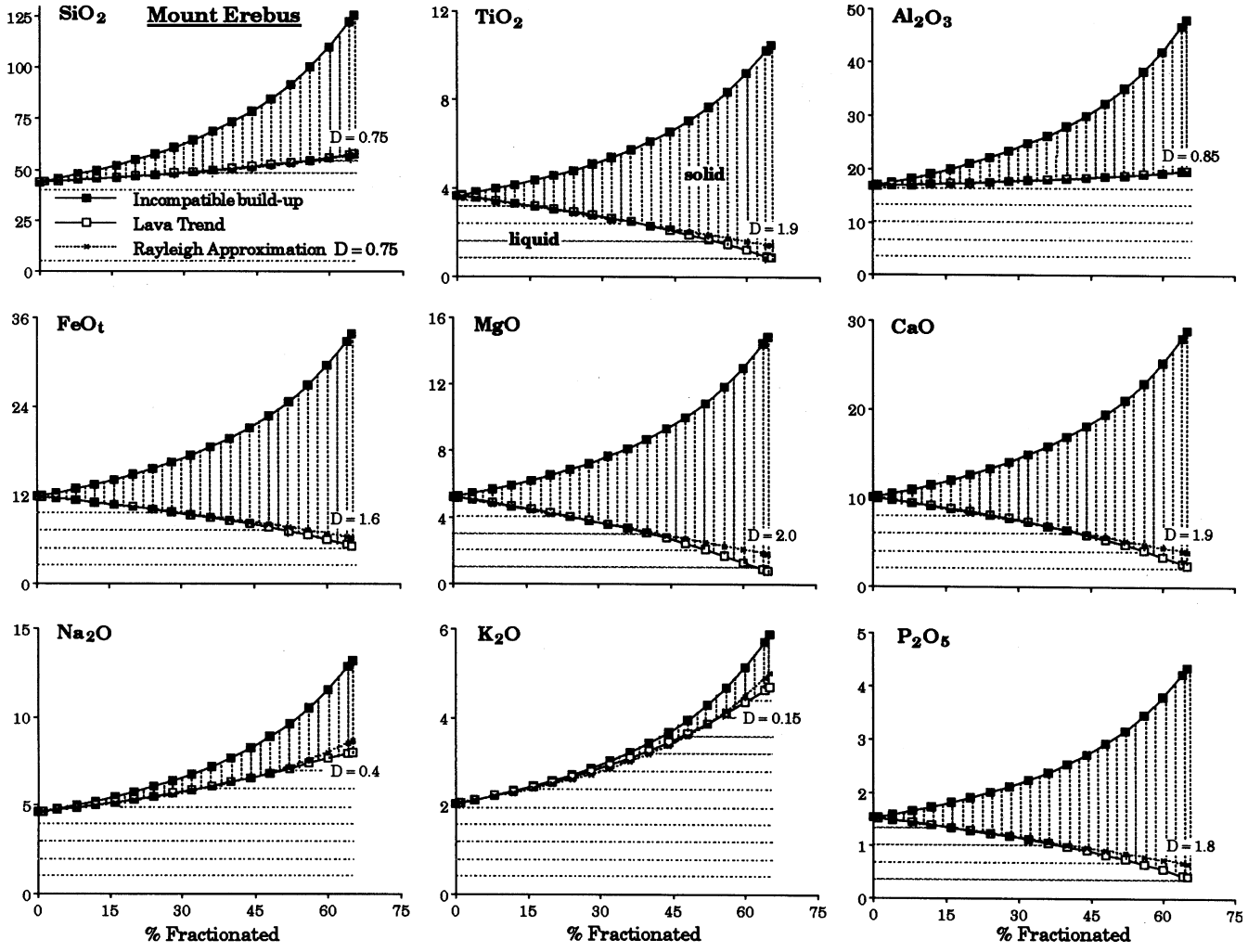

Fig. 4 Chemical variation diagrams monitored with '% fractionated' [(1-*F*)*100] for liquid and for perfect incompatible enrichment, outlining fields for each component in solid and in liquid. Rayleigh fractionation trends with constant $D^{S/L}_{oxide}$ values are superimposed for comparison. Felsic components (SiO_2, Al_2O_3, Na_2O and K_2O) have variably restricted fields of solid

and P enrichment attained in fractionation of more primitive alkaline lava sequences (e.g., Kerguelen, Indian Ocean, Yang et al. 1998; Tenerife, Canary Islands, Ablay et al. 1998; Terceira, Azores, Mungall and Martin 1996; Galapagos Islands, Ecuador, Geist et al. 1995, Naumann et al. 2002).

Oxides versus degree of fractionation

The conversion of Zr in the lavas to *F* and "% fractionated" [(1-*F*)*100] [Eq. 1; Fig. 4] provides a quantitative means to evaluate the evolution of lavas (liquids) at Mt. Erebus. The m^o_i (start of' fractionation) value of each oxide is calculated at $c^o_{Zr} = 350ppm$ in Fig. 3 (Table 2). Each oxide is portrayed on (1) hypothetical perfectly incompatible enrichment profiles and (2) liquid chemical variation profiles derived from the lavas. Sixty-five wt% of the *local starting* basanite magma was solidified, while Zr was enriched from 350 to 1,000 ppm.

The distribution of components between liquid and solids are visually distinct in Fig. 4. The positive slope of the SiO_2 liquid profile at $D^{S/L}_{SiO_2} \sim 0.75$ assures that SiO_2 will be in higher concentration in liquid than in solid. The less steep positive profile for Al_2O_3, at $D^{S/L}_{Al_2O_3} \sim 0.85$, keeps slightly more Al_2O_3 in liquid, but very steep positive profiles for Na_2O and K_2O keep most of these components in liquid. The liquid profile for MnO (not shown) is poorly constrained and flat ($D^{S/L}_{MnO} \sim 1$), but those for MgO, CaO, FeO_t, TiO_2 and P_2O_5 are strongly negative, with $D^{S/L}_{oxide}$ ranging from 1.6–2.0, and they are transferred strongly to solid. It is apparent that there are more mafic components in the solid than in the liquid in this span of fractionation from basanite to phonolite, and that the solid will be more highly silica-undersaturated than the liquid.

If solidification were to occur with significant "trapped liquid" (5–30 wt%; Barnes 1986; Kerr and Tait 1986), bulk $D^{S/L}_{Zr}$ values would increase by the same factor (0.05–0.3, MacLean 2000). This increase has the effect of extending apparent % fractionated to higher values, and leads to predictions of more highly evolved solids.

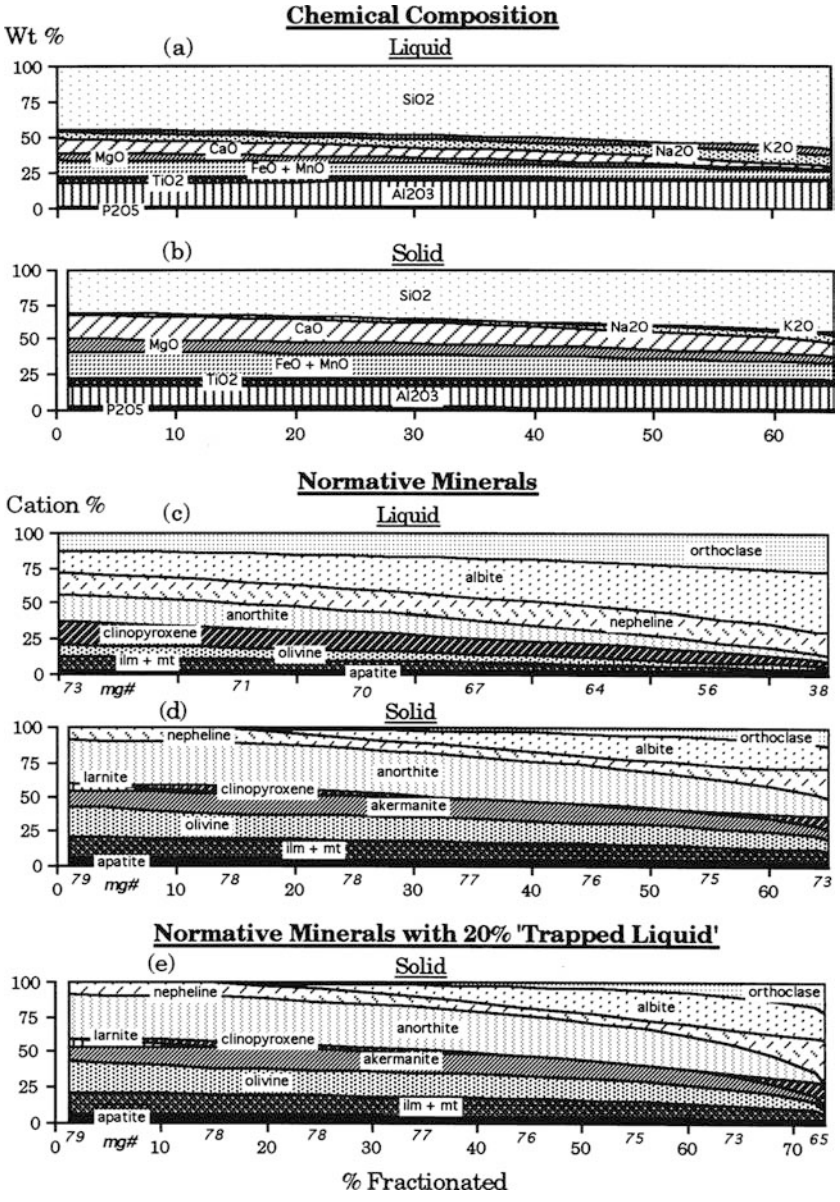

Fig. 5. a, b Area diagrams showing chemical change in liquid and in solid during fractional crystallization. The amounts of mafic components decrease gradually with fractionation in both liquid and solid, and there is obviously more mafic component in solid. **c, d** Normative mineral compositions (in cation %) of liquids and the solids. Liquids are enriched in alkali feldspar, and the solids in anorthite. Åkermanite is modeled as the main undersaturated mineral in solids. The small amount of larnite is likely to be in solid solution in olivine. Bulk mg-numbers (mg#) are in cation %, and shown in italics. *ilm*-ilmenite, *mt*-magnetite. **e** Solid formed with 20% ''trapped'' interstitial liquid. This produces a bulk $D_{Zr}^{S/L} = 0.2$ (MacLean 2000), and increases apparent fractionation from ~65 to 73% to produce a more felsic solid residue

Area plots

Area chemical variation plots (Fig. 5a, b) display a continuous history of compositional change in the Mt. Erebus liquid and estimated solid as the magma crystallizes. As fractionation proceeds, the felsic components in both liquid and solid typically become enriched and the mafic components depleted. However, as noted for Fig. 4, the ratio of mafic to felsic components is significantly higher in the solid than in the liquid.

Changes in chemical composition are also depicted with normative minerals (cation percent, Fig. 5c, d, e). Ferric and ferrous iron were estimated at $Fe\# = Fe^{3+}/Fe_{total} = 0.3$ (cation), which is somewhat above the quartz-fayalite-magnetite oxygen buffer at magmatic temperatures. Both liquid and solid contain a considerable amount of nepheline. The differences in the chemistry of liquids and solids are also seen in the normative minerals: the liquids contain ~45–85% felsic component (alkali feldspar and nepheline), and the solid ~10–50%. Anorthite, clinopyroxene, olivine, Fe-Ti-oxides and apatite are major normative components of both liquid and solid, and are reported as modal phenocryst and matrix minerals in the lavas by Kyle et al. (1992).

With Fe# = 0.3, the early-formed solid (0–40% fractionation) is still SiO_2-deficient with all alkalis expressed as felspathoid, and periclase (Mg,Fe)O and minor CaO were generated in the norm. Fractionation at lower Fe# produces more normative periclase, and enhances the problem. To produce silica to react with periclase, sufficient clinopyroxene was recalculated as the melilite-group end-member mineral, åkermanite ($Ca_2MgSi_2O_7$), in the reaction: 8Cpx + 5Per = 7Ak + 6Ol. The small amount of normative CaO was recalculated as larnite (Ca_2SiO_4): 2CaO + 10Ak = 9Lar + 3Ol. The larnite probably formed a solid solution with olivine.

Other Si-poor normative mineral options are possible. Kaersutite, $NaCa_2Mg_4TiAl_2Si_6[O_{23}(OH)]$, is a scarce amphibole in Mt. Erebus lavas (Kyle et al. 1992) and in other alkaline suites. However, it is not sufficiently Si-poor to provide sufficient SiO_2 to consume all the normative periclase in solid, and it also selectively fractionates and decouples Nb and Zr (Tiepolo et al. 2001; Hofmann 1988), a phenomenon that does not appear to have affected the HFSE in this volcanic suite (Fig. 3). Minerals of the garnet group are also Si-poor options (Eggins 1992; Huang and Wiley 1986; Boyd 1970), but none are recorded at Mt. Erebus (Kyle et al. 1992), and they too strongly fractionate HFSE.

Discussion

A study of the chemical evolution of a crystallizing magma via a suite of volcanic rocks is invariably hindered by a lack of equivalent data for solids. Differentiation profiles of liquid and solid fractions are not simple mirror images, and substitutions of one for the inverse of the other can lead to large error in interpretation. A full view of crystallized cumulate solids is rarely accessible to observation and, even when exhumed, correlation of solids with particular lavas would be difficult or impossible.

The lack of direct field study of liquid-solid relations is alleviated by calculation techniques designed to estimate the solid fraction (e.g., Kyle et al. 1992; DePaolo 1981; Bryan et al. 1969). These largely involve addition and subtraction of minerals with a chosen parental liquid, using $D^{S/L}_{oxide}$ values and mineral compositions to essentially establish a liquid line of descent. The *profile* method is designed in the opposite way: it establishes a chemical liquid line of descent from the lava suite monitored by F and, from this, the amount and chemical composition of solid is calculated with Eqs. (11) and (15). Techniques have also been designed to estimate liquid compositions from solids (e.g., Morse 1996, 1997; Chayes 1970; Wager 1960).

Error in the *profile* procedure is linked largely to sampling of lavas, analytical inaccuracies, choice of regression equations for lava sample data, changes in $D^{S/L}_{HFSE}$ for the monitoring trace element, hydrothermal alteration, and chemical weathering. Pulses of new magma injected into a holding chamber also produce scatter in chemical data, as do wall-rock contamination and trapped liquid in accumulating solids; these factors are treated in MacLean (2000). Series of fresh lava flows, particularly aphyric rocks, should produce the most accurate liquid fractionation profiles.

Improvements in accuracy and precision of bulk rock chemical analyses, particularly for the HFSE, but also for TiO_2, K_2O and P_2O_5 in low values in basalts, have alleviated many problems in the calculations. The scatter of HFSE on variation diagrams for alkaline (particularly for the ocean island and related types) and tholeiitic lavas has diminished substantially over the last decade or so, their linearity has increased, and they more commonly pass through or close to the origin of the plots (Fig. 3). Whatever the previous history of partial melting and crystallization, once a body of tholeiitic or alkaline liquid has separated from its melting source and begins to crystallize, the *incompatible* HFSE will retain their inter-HFSE ratios and produce linear enrichment arrays that project through the origin (Thompson et al. 2001; Tiepolo et al. 2001; MacLean 2000; Yang et al. 1998; Hoffman 1988). This is also true for Ti, K and P in basaltic liquid, for there they too are commonly incompatible. The HFSE are, however, commonly compatible and cannot be used to estimate F in calc-alkaline liquid, or in alkaline liquid that has been strongly contaminated by crustal rocks.

Acknowledgments I wish to thank David Dolejs and Robert F. Martin for early constructive reviews of the manuscript. I also thank journal reviewer S.A. Morse for his acute understanding of the proposed methodology, and suggestions to improve its presentation. I am also grateful to Ian Parsons for his penetrating and constructive comments on the final presentation of the manuscript. Numerous discussions with David Dolejs on problems of magma fractionation, his assistance with reference material and the drafting of some of the figures, and his help in understanding the Albaréde (1995) approach to mass-balance calculations, are deeply appreciated.

References

Ablay GJ, Carroll MR, Palmer MR, Marti J, Sparks RSJ (1998) Basanite-phonolite lineages of the Teida-Pico Viejo volcanic complex, Tenerife, Canary Islands. J Petrol 39:905–936

Albarède F (1995) Introduction to geochemical modeling. Cambridge University Press, Cambridge, 543 pp

Barnes SJ (1986) The effect of trapped liquid crystallization on cumulus mineral compositions in layered intrusions. Contrib Mineral Petrol 93:524–531

Barrett TJ, MacLean WH, Tennant SC (2001) Volcanic sequences and alteration at the Parys Mountain volcanic-hosted massive sulfide deposit, Wales, United Kingdom: application of immobile element geochemistry. Econ Geol 96:1279–1305

Beattie P (1994) Systematics and energetics of trace-element partitioning between olivine and silicate melts: implications for the nature of mineral/melt partitioning. Chem Geol 117:57–71

Boyd FR (1970) Garnet peridotite and the system $CaSiO_3$-$MgSiO_3$-Al_2O_3. Mineral Soc Am Spec Pap 3:63–75

Bryan WB, Finger LW, Chayes F (1969) Estimating proportions in petrographic mixing equations by least-squares approximation. Science 163:926–927

Chayes F (1970) On estimating the magnitude of the hidden zone and the compositions of the residual liquids of the Skaergaard layered series. J Petrol 11:1–14

Civetta L, D'Antonio M, Tilton GR (1998) The geochemistry of volcanic rocks from Pantelleria Island, Sicily Channel: petrogenesis and characteristics of the mantle source region. J Petrol 39:1453–1491

Dalpé C, Baker DR, Sutton RS (1995) Synchrotron X-Ray-Fluorescence and Laser-Ablation ICP-MS microprobes: useful instruments for analysis of experimental run-products. Can Mineral 33:481–498

DePaolo DJ (1981) Trace element and isotopic effects of combined wallrock assimilation and fractional crystallization. Earth Planet Sci Lett 53:189–202

Dunn T, Sen C (1994) Mineral/matrix partition coefficients for orthopyroxene, plagioclase and olivine in basaltic and andesitic systems: a combined analytical and experimental study. Geochim Cosmochim Acta 58:717–733

Eggins SM (1992) Petrogenesis of Hawaiian tholeiites: 1, phase equilibria constraints. Contrib Mineral Petrol 110:387–397

Geist D, Howard KA, Larson P (1995) The generation of oceanic rhyolites by crustal fractionation: the basalt-rhyolite association at Volcan Alcedo, Galapagos Archipelago. J Petrol 36: 965–982

Hack PJ, Nielsen RL, Johnson AD (1994) Experimentally determined REE and Y partitioning behavior between cpx and basaltic liquids at pressures up to 20 kb. Chem Geol 117:89–105

Hofmann AW (1988) Chemical differentiation in the Earth: the relationship between mantle, continental crust, and oceanic crust. Earth Planet Sci Lett 90:297–314

Huang WL, Wyllie PJ (1986) Phase relationships of gabbro-tonalite-granite-water at 15 kbar with applications to differentiation and anatexis. Am Mineral 71:301–316

Hunter RH (1996) Texture development in cumulate rocks. In: Cawthorn RG (ed) Layered Intrusions. Elsevier, Amsterdam, pp 77–101

Kerr RC, Tait SR (1986) Crystallization and compositional convection in a porous medium with application to layered igneous intrusions. J Geophys Res 91:3591–3608

Kyle PR, Moore JA, Thirlwall MF (1992) Petrologic evolution of anorthoclase phonolite lavas at Mount Erebus, Ross Island, Antarctica. J Petrol 33:849–875

Larson LM, Fitton JG, Saunders AD (1999) Composition of volcanic rocks from the southeast Greenland margin, Leg 163: major and trace element geochemistry. Proc ODP, Scientific Results 163, pp 63–75

MacLean WH (1990) Mass change calculations in altered rock series. Mineral Deposita 25:44–49

MacLean WH (2000) Calculation of the composition of fractionated solid as deduced from chemical profiles in tholeiitic lava. Contrib Mineral Petrol 139:85–100

MacLean WH, Barrett TJ (1993) Lithogeochemical techniques using immobile elements. J Explor Geochem 48:109–133

Mahood GA, Stimac JA (1990) Trace-element partitioning in pantellerites and trachytes. Geochim Cosmochim Acta 54: 2257–2276

Morse SA (1996) Kiglapait mineralogy III. Olivine compositions and Rayleigh fractionation models. J Petrol 37:1037–1061

Morse SA (1997) Binary solutions and the lever rule revisited. J Geol 105:471–482

Mungall JE, Martin RF (1995) Petrogenesis of basalt-commendite and basalt-pantellerite suites, Terceira, Azores, and some implications for the origin of ocean-island rhyolites. Contrib Mineral Petrol 119:43–55

Naumann T, Geist D, Kurz M (2002) Petrology and geochemistry of Volcán Cerro Azul: petrologic diversity among the western Galápagos volcanoes. J Petrol 43:859–883

Rayleigh JWS (1896) Theoretical considerations respecting the separation of gases. Philos Mag 42:493–498

Thompson GM, Smith IEM, Malpas JG (2001) Origin of oceanic phonolites by crystal fractionation and the problem of the Daly gap: an example from Rarotonga. Contrib Mineral Petrol 142:336–346

Tiepolo M, Bottazzi P, Foley SF, Oberti R, Vannucci R, Zanetti A (2001) Fractionation of Nb and Ta from Zr and Hf at mantle depths: the role of titanian pargasite and kaersutite. J Petrol 42:221–232

Wager LR (1960) The major element variation of the Layered Series of the Skaergaard Intrusion. J Petrol 1:364–398

Yang H-J, Frey FA, Weis D, Giret A, Pyle D, Michon G (1998) Petrogenesis of the flood basalts forming the northern Kerguelen Archipelago: implications for the Kerguelen Plume. J Petrol 39:711–748